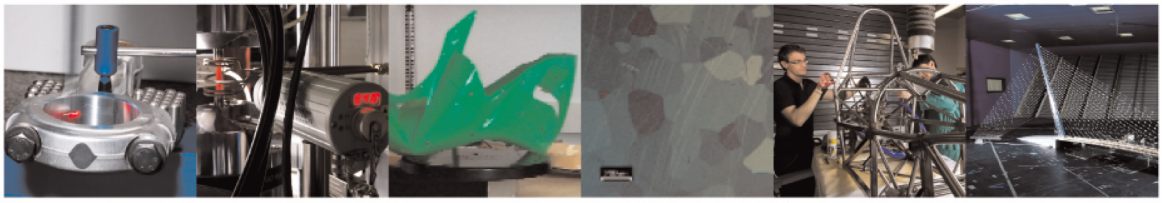

An investigation about the influence of deep rolling on fatigue crack growth in railway axles made of a medium strength steel

D. Regazzi, S. Beretta, M. Carboni

This is a post-peer-review, pre-copyedit version of an article published in Engineering Fracture Mechanics. The final authenticated version is available online at: http://dx.doi.org/10.1016/j.engfracmech.2014.09.016

DIPARTIMENTO DI MECCANICA ■ POLITECNICO DI MILANO
via G. La Masa, 1 ■ 20156 Milano ■ EMAIL (PEC): pecmecc@cert.polimi.it
http://www.mecc.polimi.it
Rev. 0

An investigation about the influence of deep rolling on fatigue crack growth in railway axles made of a medium strength steel

D. Regazzi, S. Beretta, M. Carboni *

Dept. Mechanical Engineering, Politecnico di Milano, Via La Masa 1, 20156 Milano, Italy

Article history:
Received 17 December 2013
Received in revised form 1 August 2014
Accepted 29 September 2014
Available online 7 October 2014

1. Introduction

Railway axles are usually designed against the fatigue limit [1,2], but, due to their very long service life (30 years or 10^7 km) and to in-service damages like corrosion [3,4] or ballast impacts [5], the traditional design is complemented by a damage tolerant approach [6–8]. From this point of view, the presence of cracks in running axles is accepted and they must be periodically inspected by non-destructive testing (NDT) methods. The problem so switches to the determination of the appropriate inspection interval, based on crack growth life predictions and the adopted non-destructive testing technique [9]. Usually, a 2 mm deep initial defect, which corresponds to a conservative assumption for the damage induced by ballast hits [5], is adopted. Simulations of crack propagation are then performed, based on the knowledge of several factors as the crack propagation behavior of the material, the in-service loads acting on the component and the stress intensity factor (SIF) of the considered geometries. After the estimation of crack growth life, the inspection interval is defined by calculating the failure probability of the axle starting from the "Probability of Detection" (POD) curve of the adopted NDT method [10] (an alternative method is to define the NDT specifications for a chosen length of the inspection interval [11]).

Considering the possible methods to improve crack growth life of mechanical components subjected to fatigue, several surface mechanical procedures have been more and more adopted [12–15], over the last few decades, to increase their

* Corresponding author. Tel.: +39 02 23998253; fax: +39 02 23998202.
E-mail address: michele.carboni@polimi.it (M. Carboni).

Nomenclature

a	crack depth
a_0	initial crack depth
c	surface semi-crack length
c_0	initial surface semi-crack length
A–D	parameters of the Shiratori weight function
K_0–K_3	contributions to the SIF due to the ith polynomial approximation
K_I	mode I SIF
M	dimensionless SIF
R	stress ratio
t	thickness of the plate
Δa	crack depth increment
Δc	surface semi-crack length increment
ΔK	SIF range
ΔK_{max}	maximum SIF range applied at the beginning of a given test and corresponding to the highest stress level of the stress spectrum
ΔK_{th}	threshold SIF range
Φ	elliptical integral for the Shiratori weight function
σ_0	nominal stress
σ_{max}	maximum stress level of the load spectrum

service durability and reliability. Nevertheless, while some scientific analyses were recently dedicated to the investigation of the beneficial effects of compressive residual stresses onto fatigue life [16–19] and crack propagation [20–24] in specimens made of aluminum and steel, no investigations were found in the literature about the effects of deep rolling onto fatigue crack propagation in real components. Since deep rolling is the technological process traditionally adopted by axle producers, and the damage tolerant approach is the design methodology, the focus was here pointed onto this particular procedure for life extension of railway axles. Deep rolling [25] is basically performed pressing a roller against the rotating axle and applying a certain amount of pressure in order to induce plastic deformation at the surface and, consequently, the compressive residual stresses. The roller translates along the whole surface of the axle or just along those regions where compressive residual stresses are required. The relevant technological parameters, depending on the desired magnitude of residual stresses and their maximum depth, are the geometry of the roller at the contact region, the longitudinal feed (i.e. the step of advancement along the axle) and the applied contact force [25].

In order to deepen the subject, the MARAXIL (“Manufacturing Railway Axles With Improved Lifetime”) Project, supported by Regione Lombardia (Italy) [26], was launched in order to experimentally and theoretically investigate the effect of deep-rolling onto the in-service life of railway axles made of EA4T steel, one of the standardized grades [1,2] for the production of axles.

Compressive residual stresses, in addition to the typical rotating bending stress state, modify the in-service stress ratio of axles from the typical value ($R = -1$) to the very negative region ($R = 10$ or even below). For this reason, the crack propagation behavior of the material, in the unexplored region of the very negative stress ratios, was firstly experimentally characterized.

In order to verify the enhancement in propagation lifetime, full-scale specimens were designed for variable amplitude (VA) crack propagation tests on a test bench with a 250 kNm capacity: three full-scale crack growth tests were performed considering different initial notch depths.

Full-scale experimental results were compared to simulated predictions carried out by a crack propagation algorithm, where residual stresses were superimposed to bending ones and crack growth rate was modeled by Nasgro’s propagation equation [27].

2. Characterization of the material to crack propagation

The material considered in this study is the EA4T (quenched and tempered 25CrMo4) steel grade, one of the standardized steels used for the production of railway axles [28] running in Europe.

Due to the superposition of the very high compressive residual stresses, expected as the consequence of the deep-rolling technological process, and the stresses due to the in-service rotating bending, the stress ratio acting at the surface of the axle will be different, in particular much lower, than the typical $R = -1$ value due to rotating bending alone. From this point of view, a dedicated experimental campaign was carried out, in order to investigate the crack propagation behavior of the A4T grade in the not-yet-explored region of very negative stress ratios. In particular, two different shapes of specimen were tested:

- 12 × 24 mm SE(B) specimen with an 8 mm initial notch length obtained by electro-discharging manufacturing (EDM), 12 samples;
- 20 × 50 mm SE(T) specimen with a 7 mm initial notch length obtained by EDM, 4 samples.

As known from the literature [29–32], the traditional experimental technique (ΔK-decreasing, [33]) for generating threshold SIFs overestimates their values. For this reason, all the adopted specimens were prepared using the compression pre-cracking approach [32,34–36].

Crack propagation tests onto SE(B) specimens were carried out using a Rumul Craktronic resonant plane bending facility working at a frequency equal to about 130 Hz. A total of 12 SE(B) specimens were tested at different stress ratios ranging from $R = 0.7$ to $R = -2.5$. At every considered stress ratio, both the crack growth rate and the threshold SIF were investigated by means of the "Compression Pre-cracking Constant Amplitude" (CPCA) [35] and the "Compression Pre-cracking Load Reduction" (CPLR) [30] tests, respectively. In order to obtain relevant results for even more negative stress ratios, a total of four SE(T) specimens were tested by a servo-hydraulic mono-axial facility, instrumented with a 250 kN load cell, at different stress ratios ranging from $R = -2.5$ to $R = -4$.

Fig. 1a shows the obtained experimental fatigue crack growth curves together with their interpolations carried out adopting the Nasgro equation [27] and the maximum likelihood method [37]. The same diagram also shows a comparison to the interpolation of experimental data [38] obtained by the traditional ΔK-decreasing approach for the same material. It is worth noticing the tendency of data to overlap at very negative stress ratios: all the tests carried out at $R \leqslant -2$ collapsed on the experimental data obtained at $R = -2$, suggesting a stabilization of the crack propagation behavior of the considered material at very negative stress ratios. This is also in agreement with the declared validity of the Nasgro equation for thresholds [27] over the stress ratio range $-2 \leqslant R \leqslant 0.7$.

Fig. 1b shows the trend of the ΔK_{th} against the stress ratio, as obtained from the present experimental campaign, and compares it to data from the literature [38] obtained by the application of the ΔK-decreasing technique to the same material.

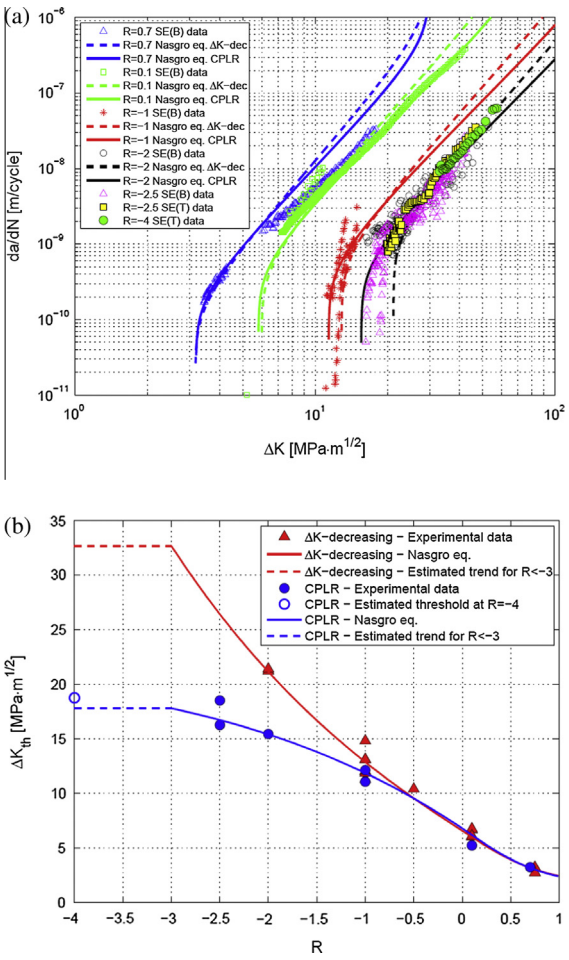

Fig. 1. Crack growth behavior of EA4T steel grade: (a) crack growth curves; (b) trend of the threshold SIF range with stress ratio.

Experimental data were interpolated by the Nasgro equation for thresholds [27], adopting, again, the maximum likelihood methodology. It is evident that the compression pre-cracking technique results in lower threshold SIF ranges when compared to the traditional approach and that such a difference significantly increases decreasing the stress ratio. Threshold values (Fig. 1b) and crack growth curves for $R < -3$ were considered constant, based on the observations onto Fig. 1a.

3. Full-scale test details

3.1. Specimens and test details

The adopted full-scale specimen, shown in Fig. 2a, was specifically designed, according to the relevant standard [28], for the three point rotating bending bench (Fig. 2b), having capacity 250 kNm, available at Politecnico di Milano – Dept. Mechanical Engineering. A portion of such a specimen, characterized by a lowered diameter equal to 130 mm, was subjected to the particular deep-rolling procedure used to produce deep-rolled axles for high-speed applications in Europe. In particular, the lower diameter of the deep-rolled portion of the specimen was adopted to overcome the high compressive residual stresses and to allow for crack propagation.

After deep rolling, two semi-circular artificial defects were introduced, by EDM and at 180° to each other, into the deep-rolled portion of each specimen. In particular, three specimens were prepared, differing for the initial artificial notch radius: 2 mm, 3 mm and 4 mm. These particular dimensions were chosen based on the residual stress profiles measured according to Section 3.2.

Specimens were then subjected to both Constant Amplitude loadings (CA) and VA sequences, derived from a typical in-service load spectrum available in the literature [39] and representative of about 57,000 km of high-speed service. The normalized load spectrum and its discretization in load blocks are shown in Fig. 3a. The magnification of stress levels was set to obtain the equivalence, in terms of crack driving force, between the specimen and the real in-service axle, both containing 2 mm defects. This resulted in a maximum ΔK value, applied at the beginning of the given test and corresponding to the highest stress level of the stress spectrum, equal to 16.70 MPa$\sqrt{}$m. Such a magnification, corresponding to a maximum amplitude stress level of 165 MPa at the notched section, will be called "100% amplitude" in the following. Moreover, all the stress levels below the stress value corresponding to a ΔK (calculated considering the smaller notch size) of about 50% of the expected ΔK_{th} were cut. This allowed reducing the length of the spectrum to about 41,000 cycles, nevertheless preserving the correspondence with the original mileage. Finally, the discretized blocks were arranged in the block load sequence shown in Fig. 3b.

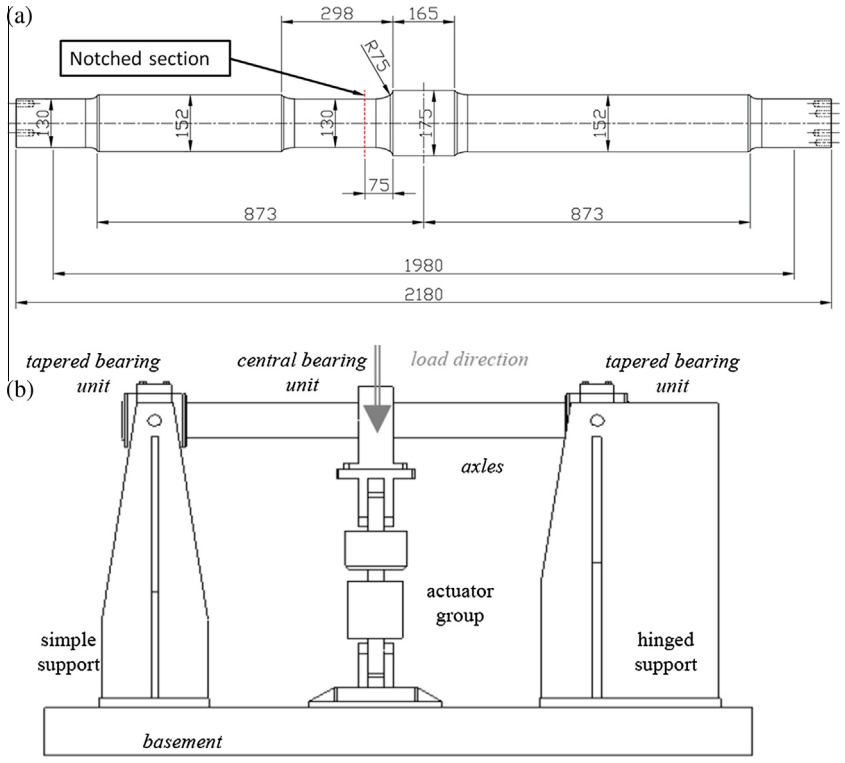

Fig. 2. Experimental set-up for testing full-scale deep-rolled specimens: (a) drawing of the specimen; (b) scheme of the three point rotating bending facility.

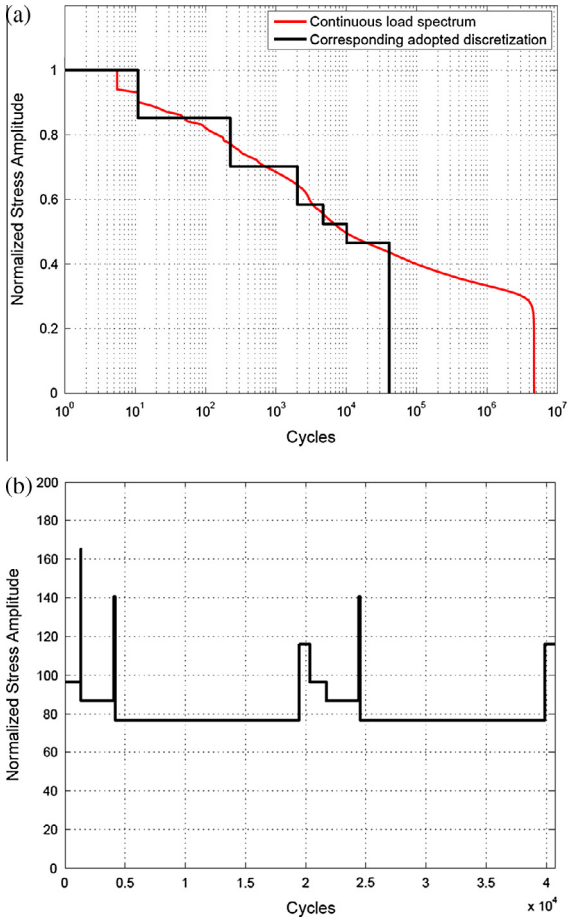

Fig. 3. Applied load spectrum, in terms of stress amplitudes, adopted for testing the full-scale specimens: (a) normalized block load spectrum, against the continuous original spectrum; (b) applied block load sequence (100% amplitude).

Actually, the shape of developing cracks immersed into a residual stress field is not very well known, so, during full-scale tests, the monitoring of crack growth was carried out using both visual (by an optical microscope and plastic replicas [40]) and ultrasonic (single crystal and phased array approaches) testing. In particular, visual testing (VT) was applied to monitor any possible propagation at the surface and at the internal bottom of the artificial notches, while phased array ultrasonic testing (PAUT, S-Scan, 32 active elements, 5 MHz) to monitor in-depth crack tip propagation by means of the "crack tip diffraction" method [41]. Traditional single-crystal ultrasonic testing (UT, 4 MHz, 45°) was, instead, applied to monitor the general increase of the dimension of the defects by acquiring the amount of reflected sound energy in terms of gain needed to get the amplitude of the signal response up to the 90% of the screen of the flaw detector unit.

In the following, the characterization of the residual stress profiles, before and after the full-scale crack growth tests, is firstly given, followed by the description of the full-scale tests themselves.

3.2. Measurement of the residual stress profile in full-scale specimens

The residual stress profile was experimentally derived by X-ray diffraction (XRD [42,43]) in order to quantify its longitudinal and circumferential components. In particular, an AST X3000 X-ray diffractometer was used. Before each crack propagation test, three different sections of the deep-rolled region of each specimen, one of which containing the artificial notches (Fig. 4a), were measured at three different surface points (0°, 120° and 240°), so not to introduce stress raisers and initiate unwanted cracks. The same sections and points were measured again at the end of the tests to understand whether the fatigue phenomenon could influence the amount of residual stresses.

The surface residual stresses along the length of the axle resulted to be uniform, section-by-section, and equal, in the section containing the artificial notches, to about −600 MPa along the longitudinal direction (see Fig. 4a about the example of the specimen containing 2 mm notches) and about −300 MPa along the circumferential one. Such a magnitude of residual stresses suggests an effective prospective action against crack propagation in full-scale axles, where, usually, the maximum

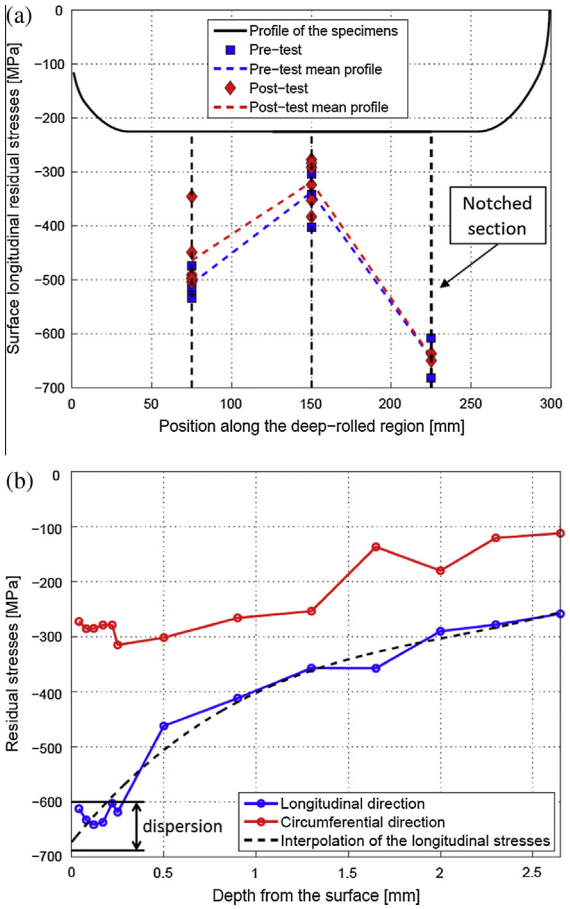

Fig. 4. Residual stress profiles into the full-scale specimen containing 2 mm notches: (a) at the surface, before and after the crack propagation test; (b) in-depth measurement, along the notched section, at the end of the test.

in-service stress amplitude is lower than 200 MPa. Moreover, the applied fatigue cycles were not able to modify the residual stress field (Fig. 4a), since the mean profile after the test remained comparable to those before the test itself.

At the end of fatigue tests, some of the measuring spots were also investigated, again by XRD, to determine the in-depth residual stress profile. In particular, slices of material, of about one tenth of millimeter, were locally and progressively removed by electro-polishing, using a solution of acetic acid (94%) and perchloric acid (6%), in order not to affect the pre-existing stress field. The residual stress patterns were determined down to a 2.5 mm depth. Fig. 4b shows, as an example, the residual stress patterns of the section containing the 2 mm artificial notches: it has to be underlined that all the specimens showed an analogous behavior. It clearly appears that the residual stresses tend to decrease rapidly close to the surface. Unfortunately, it is not possible to investigate residual stresses, by XRD, for depths larger than 2–2.5 mm, so it was here assumed that the compressive residual stresses, due to deep rolling, vanish at about 3 or 4 mm based on the trend of the measurements and the dedicated finite element analyses described in [44]. This assumption also explains the choice made about the size of the initial notches.

4. Results of full-scale tests

4.1. Results of crack propagation from 2 mm notches

The obtained XRD measurements show that 2 mm defects were completely immersed into the compressive residual stress field. The first part of the test then consisted in subjecting the specimen to a constant amplitude load generating 125 MPa at the notched section. This stress level corresponds to a ΔK value of 12.65 MPa$\sqrt{}$m at the bottom of the notches, slightly higher than the threshold SIF range at $R = -1$ as shown in Fig. 1b.

Ten million cycles were applied and no crack growth could be observed at both the surface and the deepest point of the notches. The specimen was then subjected to the 100% amplitude block load sequence shown in Fig. 3b. Such a block load sequence was applied for 2.73 million cycles, corresponding to approximately 4×10^6 km, and, since no crack propagation

Table 1
Experimental plan applied to the tested specimens.

Specimen	Test	Equivalent distance (km)	Cycles	σ_{max} (MPa)	ΔK_{max} (MPa$\sqrt{}$m)	Crack propagation	Δa (mm)	Δc (mm)
Specimen #1	CA	–	10×10^6	125		No propagation	0.1	0.1
a_0 = 2 mm	VA 100%	4×10^6	2.73×10^6		16.70	No propagation	–	–
	VA 125%	3.5×10^6	2.62×10^6		20.88	No propagation	–	–
Specimen #2	VA 100%	2×10^6	1.43×10^6		20.72	No propagation	0.1	0.1
a_0 = 3 mm	VA 125%	2×10^6	1.43×10^6		25.90	No propagation	–	–
	VA 150%	2.2×10^6	1.57×10^6		31.08	No propagation	–	–
	VA 175%	4.9×10^6	3.50×10^6		36.26	Initiation of cracks from notches	0.3	0.1
	VA 200%	5×10^6	3.57×10^6		41.44	Stable crack propagation, at both artificial notches, until final failure of the specimen	1.2	0.8
Specimen #3	VA 100%	3.5×10^6	2.60×10^6		23.80	Stable crack propagation, at both artificial notches	1.0	0.15
a_0 = 4 mm								

was again detected, its stress levels were increased by 25%, corresponding to a maximum SIF equal to 20.88 MPa$\sqrt{}$m, for another equivalent distance equal to approximately 3.5×10^6 km. All the details of the test are collected in Table 1.

In the end of this part of the test, the 2 mm notches showed, by visual testing, the presence of very short cracks. In particular, Fig. 5a shows, as an example, the state of one of the surface tips of one of the notches. As can be seen, the dimension of the observed surface cracks could be quantified in an average value equal to about 0.1 mm. On the other hand, both UT (Fig. 5b) and PAUT (Fig. 5c and d) suggested no propagation at all. This fact can be explained noticing (Fig. 5b and d) that 0.1 mm is a variation of the radius of the defect smaller than the intrinsic standard deviation of the applied UT and PAUT procedures.

Finally, the axle was suitably broken in order to observe, by the scanning electron microscope (SEM), the surface of the initial notches. Indeed, the whole edge of the notches (Fig. 5e shows an example) confirmed the onset of a very small crack. Actually, no cracks would have been expected from simulations (see Section 5), but probably they can be interpreted as non-propagating cracks likely due to the local relaxation of the compressive residual stresses owing to the machining of the notches themselves in the pre-existing compressive stress field.

4.2. Results of crack propagation from 3 mm notches

The axle containing 3 mm notches was tested because this depth roughly corresponds to the vanishing of the residual stresses due to deep rolling, see Section 3.2 and Fig. 4b.

The focus was here particularly pointed to variable amplitude loading, considering the already adopted and described load spectrum. The test started with the application of the 100% amplitudes, where the maximum stress level was, again, 165 MPa, corresponding to a 20.72 MPa$\sqrt{}$m maximum SIF range. Since no crack growth was observed after two equivalent million kilometers, the amplitude of the spectrum was gradually increased until crack propagation occurred. All the details about the experiment are reported in Table 1. For each load amplitude, a minimum distance of about two equivalent million kilometers was applied, in order to allow for any possible crack growth. As can be observed from Table 1, the maximum SIF range acting at the bottom of the crack was always higher than the threshold at $R = -1$.

The developing cracks were periodically inspected, using again the described VT, UT and PAUT techniques, at suitable test interruptions. Considering, as an example, a tip of one of the notches, Fig. 6a and b show its surface condition at the end of the 175% amplitude block load sequence and after four million cycles of the 200% amplitude one, respectively. It is interesting to notice that, around the notch, the material yielded considerably. This suggests that the rotating bending stresses were very high around the notch, but also that the residual stress field was very effective in avoiding initiation and propagation of fatigue cracks, at least up to a magnification of the load levels equal to 175%. It is also worth observing the very complex crack damage pattern: three different initiation sites can be seen in Fig. 6a (two at the corners of the notch and one along its lateral edge), but just one developed in a propagating crack (Fig. 6b) which also showed branching.

As can be seen from Fig. 6c, UT does not seem very effective to investigate crack propagation, since no significant differences could be observed over the whole test, a part for the final fracture of the specimen. A crack advance could, instead, be clearly measured (Fig. 6d) by PAUT, starting from the second half of the 175% amplitude block load sequence. This was in accordance with the just described optical measurements.

At the end of the test, one notch had developed a large crack, taking the specimen to failure, while the other one showed a small crack advance. The specimen was, then, properly cut and broken in liquid nitrogen, in order to observe the shape of

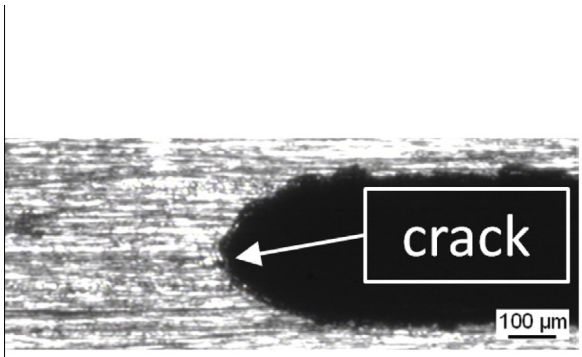

(a)

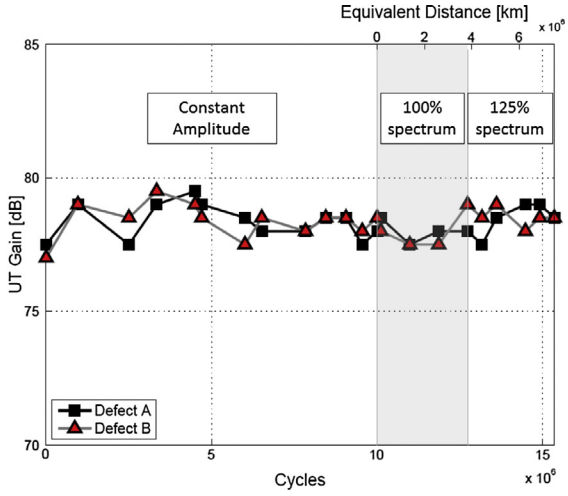

(b)

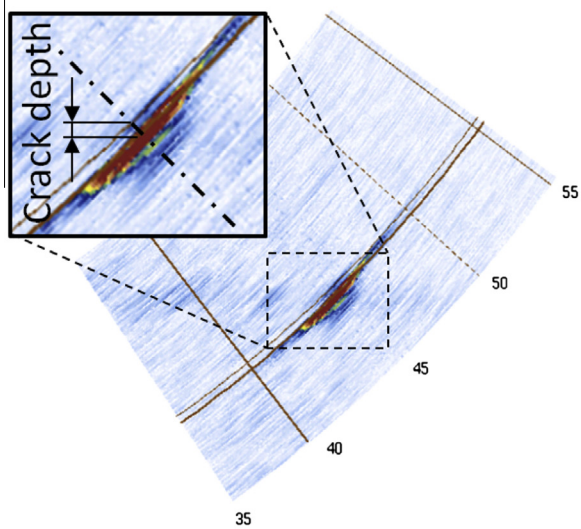

(c)

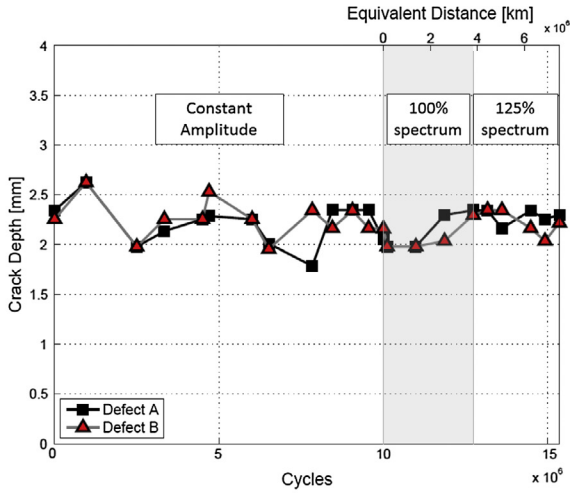

(d)

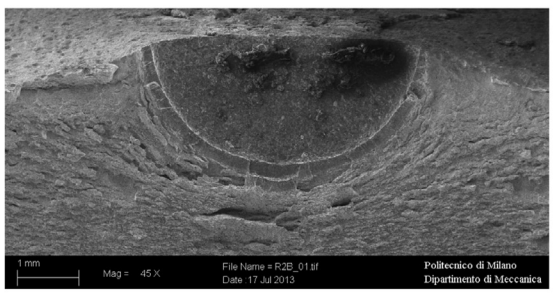

(e)

Fig. 5. Monitoring of crack growth during the full-scale test on 2 mm artificial notches: (a) visual inspection of the surface tip of one of the artificial notches (end of the test); (b) response in terms of reflected sound energy during the test; (c) example of crack depth measurement from a PAUT acquisition; (d) trend of the crack depth during the test; (e) SEM fractography of one of the 2 mm notches at the end of the fatigue test.

both the developed cracks. An optical observation of the bigger crack is shown in Fig. 7a. Beach marks, indicating particular events during the block-loading test, are evident. Particularly, the observed crack has not the typical semi-elliptical shape due to rotating bending, but tended to remain closed, during propagation, at the free surface of the axle. This means that the crack propagated faster along the depth direction, due to the presence of compressive residual stresses at the surface.

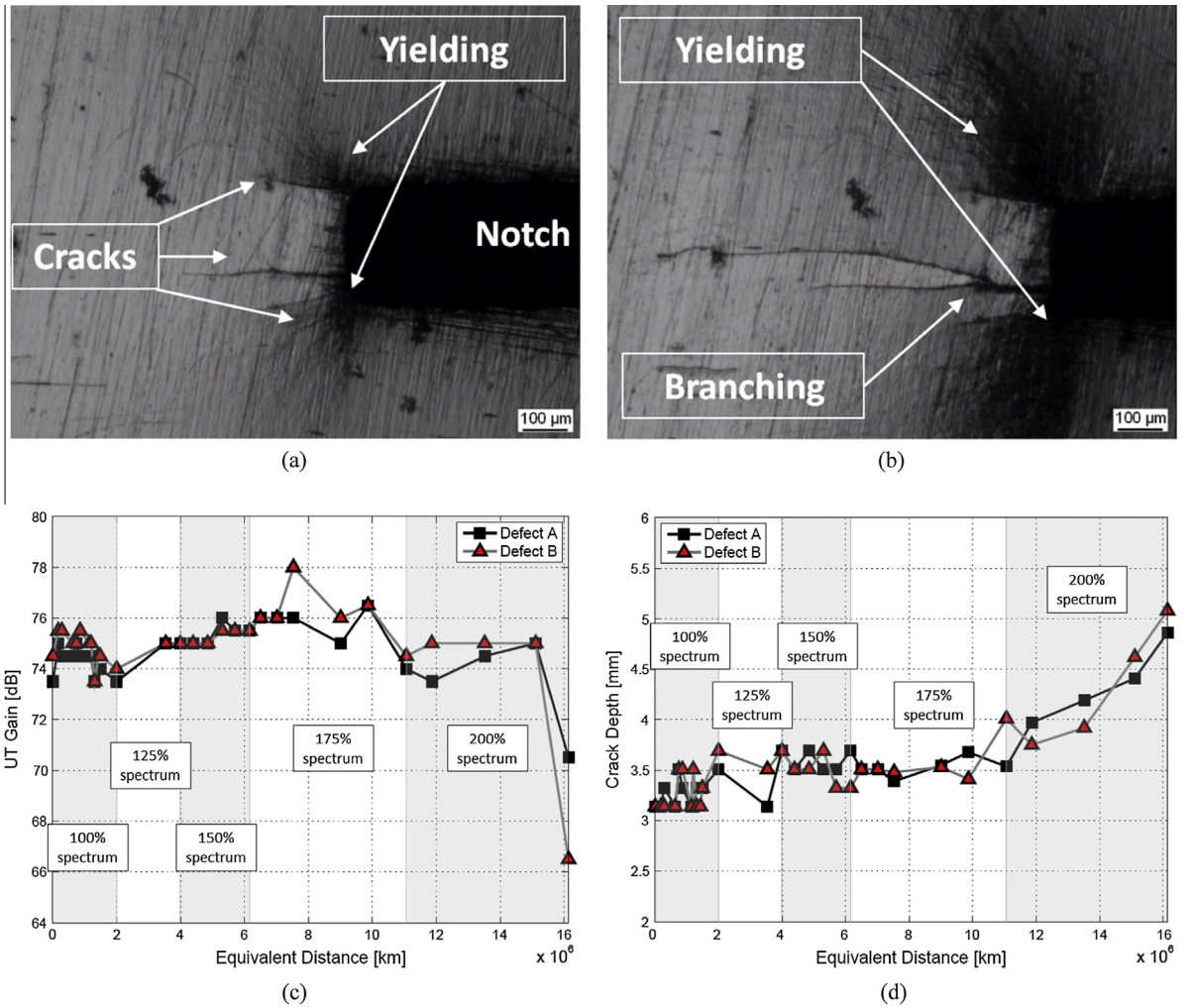

Fig. 6. Monitoring of crack growth during the full-scale test on 3 mm artificial notches: (a) condition of one of the tips of the notches at the end of the 175% amplitude block load sequence; (b) condition of the crack tip shown in a after about four million km at 200% amplitude block load sequence; (c) monitoring by UT over the whole test; (d) estimation of crack depth by PAUT over the whole test.

A SEM observation of the smaller crack is shown in Fig. 7b. This image confirms the crack shape development: the crack is bigger at the deepest point than at the free surface. Moreover, the appearance of the crack close to the notch edge reveals the same morphology of the 2 mm notch after the test, suggesting the development of an initial non-propagating crack.

4.3. Results of crack propagation from 4 mm notches

The full-scale specimen containing initial 4 mm notches was tested just using the 100% amplitude block load sequence, as in Table 1. This stress amplitude corresponded, due to the 4 mm crack depth, to a maximum SIF range of about 23.8 MPa$\sqrt{}$m. The aim of this experiment was to check the effectiveness of deep rolling against crack propagation considering the worst scenario of a quite deep crack, i.e. exceeding the depth of residual stresses. The test lasted for 64 repetitions of the block load sequence, corresponding to an equivalent distance of about 3.5×10^6 km, and was interrupted before the failure of the specimen. The notches were again monitored by both VT, UT and PAUT techniques: Fig. 8a and b show the surface condition, via optical observation of plastic replicas, at the 17th and the 64th repetitions of the block load sequence, respectively. As can be seen, developing surface cracks were found, but they advanced for a limited distance and showed an interesting behavior: they became non-propagating after about 35 repetitions of the block load sequence (Fig. 8c). This can be again explained considering the local relaxation of compressive residual stresses due to the introduction of the notches. Moreover, as for the case of 3 mm notches, two cracks initiated at each notch tip, suggesting again a peculiar and complex damage pattern due to the presence of deep-rolling residual stresses.

Considering UT, Fig. 9a shows the amount of reflected sound energy over the whole test. The trend is slightly decreasing suggesting the presence of propagation, but it is also clear the energy variation is quite small and this method is, again, not

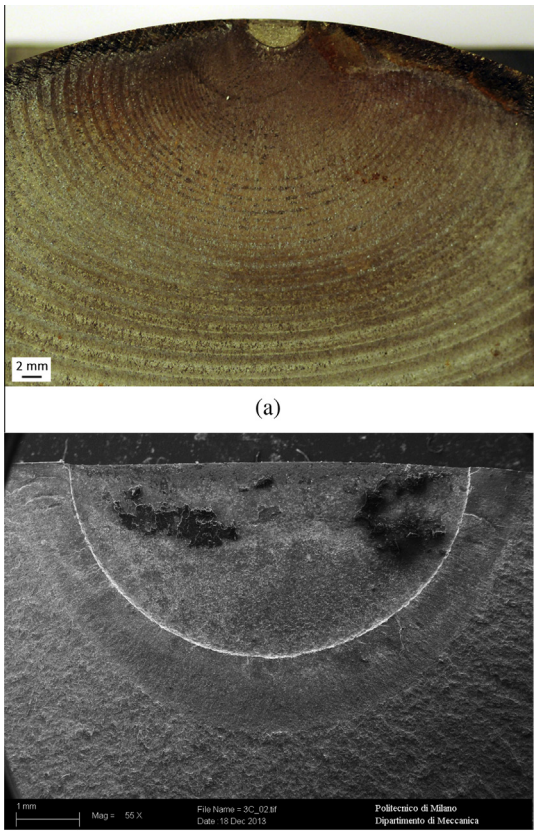

Fig. 7. Fracture surfaces of the cracks, originated by 3 mm notches, at the end of the propagation test: (a) optical observation of the bigger crack; (b) SEM observation of the smaller crack.

very effective. Measurements by PAUT resulted to be more interesting and sizable: Fig. 9b shows the experimental estimation of cracks depth. As can be seen, both cracks propagated up to about 5 mm during the whole test. This suggests again that the shape of cracks, during propagation in the residual stress field, does not likely correspond to the expected one from classical rotating bending fatigue.

5. Crack growth lifetime predictions of full-scale specimens

A simple "no interaction" (i.e. not keeping into account for load interaction effects) crack propagation algorithm was developed [45] using Shiratori's weight functions [46] for SIF determination. The SIF solution, valid for a semi-elliptical crack in a thick plate subjected to a known stress state, proved to give reasonable results also when applied to full-scale axles containing a typical semi-circular fatigue crack [47].

The SIF values were evaluated at both the deepest point (point A) and the free surface (point C) of the cracks, in order to observe the variation of crack shape. The value of the dimensionless SIF is given in tabular form [46] at both points A and C for the interpolating polynomials of the applied stress up to the third order. In particular, four dimensionless crack ratios a/t (0.2, 0.4, 0.6 and 0.8), with "a" being the crack depth and "t" the thickness of the plate, and four aspect ratios a/c (0.2, 0.4, 0.6 and 1.0), with "c" being the semi-surface length, were considered by Shiratori. During the present lifetime simulations, the dimensionless SIF M defined in Eq. (1) was evaluated by interpolation, considering the stress profiles for rotating bending and residual stresses, in order to determine the K_0–K_3 parameters reported in Eq. (2):

$$M = \frac{K_I}{(1/\Phi)\sigma_0\sqrt{\pi a}} \tag{1}$$

$$K_I = AK_3 + BK_2 + CK_1 + DK_0 \tag{2}$$

SIF values were independently determined for the two different stress conditions and then superimposed. For determining the SIFs in the prospective crack plane, the experimental longitudinal residual stress profile along the depth, described in Section 3.2, was considered and properly interpolated (Fig. 4b). The stresses due to rotating bending were instead

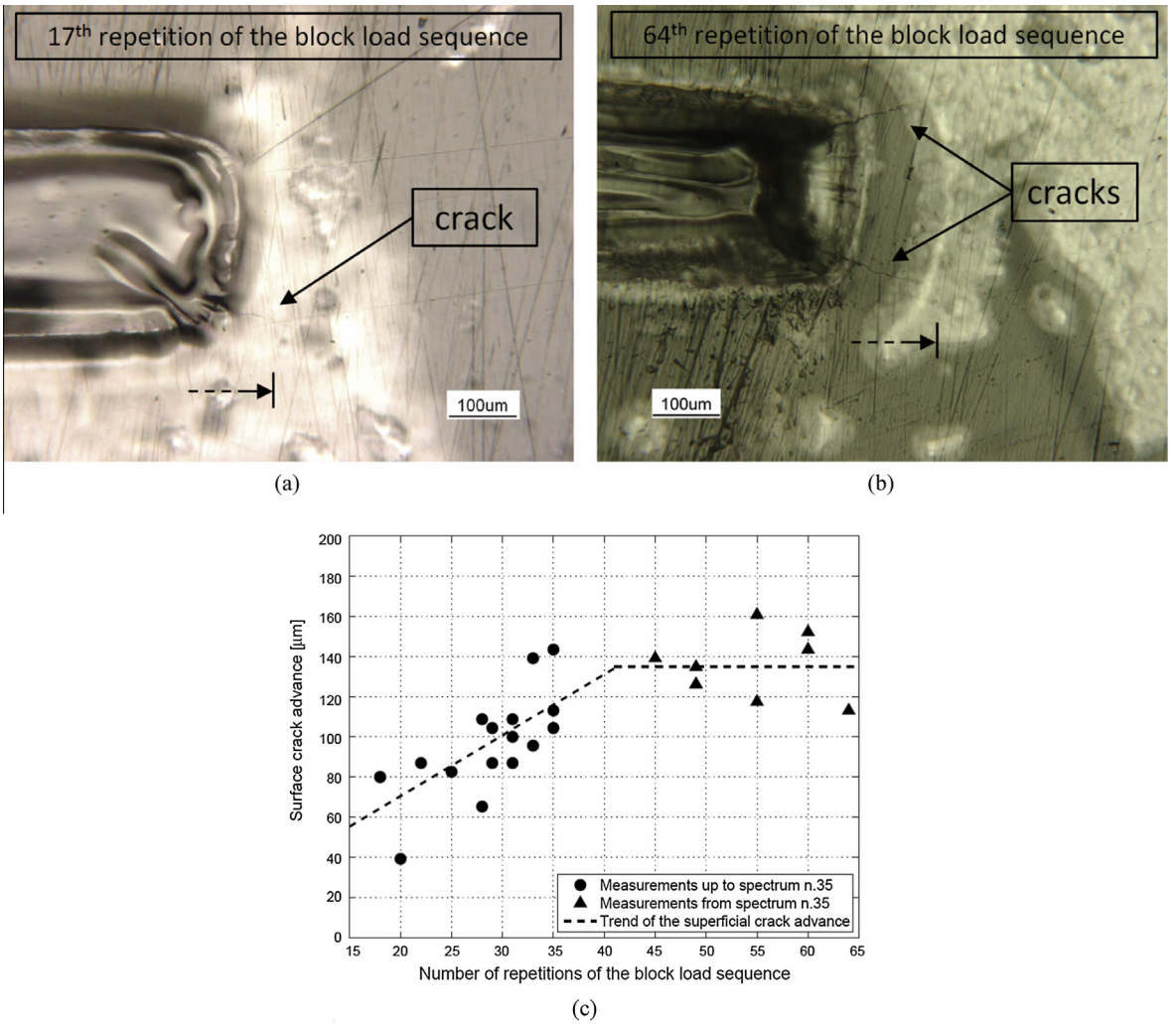

Fig. 8. Monitoring of crack growth during the full-scale test on 4 mm artificial notches: (a) appearance of one of the tips of defect B at the end of the 17th repetition of the block load sequence; (b) appearance of the crack tip shown in a at the end of the 64th repetition of the block load sequence; (c) trend of the surface crack advance, during the test.

determined by the dedicated finite element (FE) model shown in Fig. 10a. In particular, a 3D solid model was built, taking advantage of all the possible symmetries. Hinge-roller constraints were defined at the bearings, while the load was applied in the middle section of the central press-fit seat. A structured mesh was built, consisting in 20-node hexahedral elements with reduced integration, having global dimension 10 mm but reduced to about 1 mm along the deep-rolled portion of the axle. Results are shown as the nodal average of the values extrapolated from Gauss quadrature points.

The rotating bending longitudinal stress profile along the prospective crack plane was derived (Fig. 10b) and, again, suitably interpolated for the application of Shiratori's solution. Several crack growth simulations were carried out, considering all the different initial notch sizes of the tested specimens and using the same block load sequences of the experiments. In particular, the block load sequences were repeatedly applied up to failure or to the natural end of the corresponding test.

Fig. 11a–c show the estimated crack growth predictions compared to experimental outcomes for 2, 3 and 4 mm initial notches, respectively. Results of crack growth simulations are also collected in Table 2. In particular, Fig. 11a shows that a 2 mm notch, completely immersed in the compressive residual stress field due to deep rolling, is not able to propagate, at least under the considered load levels. This conclusion is in agreement with the experimental outcome. It is also worth noticing that a specimen without deep rolling would have failed during the test at CA. It can be concluded that deep rolling actually has an important influence on crack growth life of axles.

Fig. 11b shows the obtained crack propagation predictions for the 3 mm initial notch. In this case, the positive influence of deep rolling is evident, too. Moreover, ΔK-decreasing data provide longer crack growth predictions than CPLR ones. Nevertheless, the best match to experimental results is achieved, by both techniques, at the beginning of the test, while some divergence is observed toward the final part. It remains that simulations are always conservative with respect to

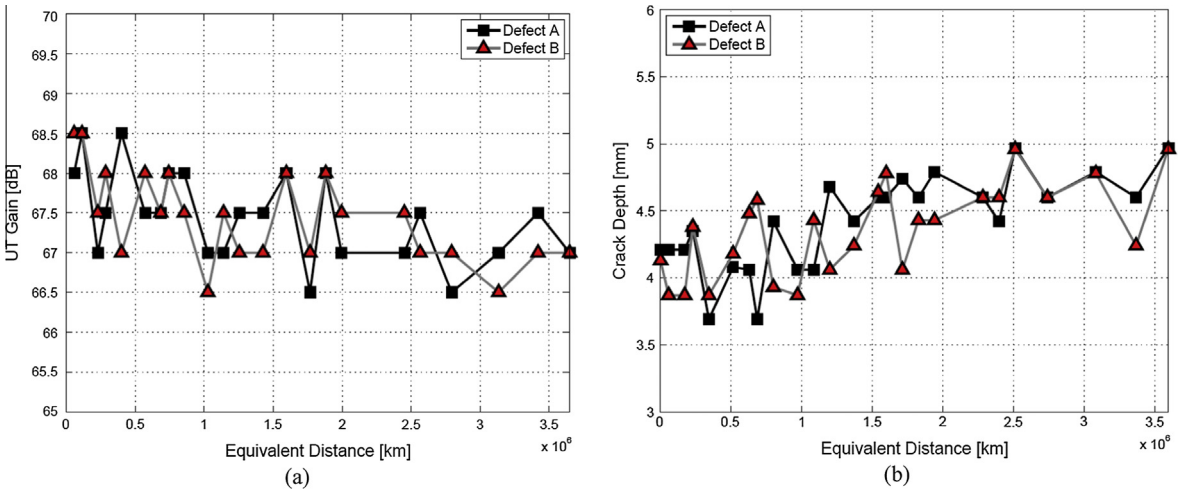

Fig. 9. Measurements of crack growth from 4 mm notches; (a) monitoring by UT over the whole test; (b) estimation of crack depth by PAUT over the whole test.

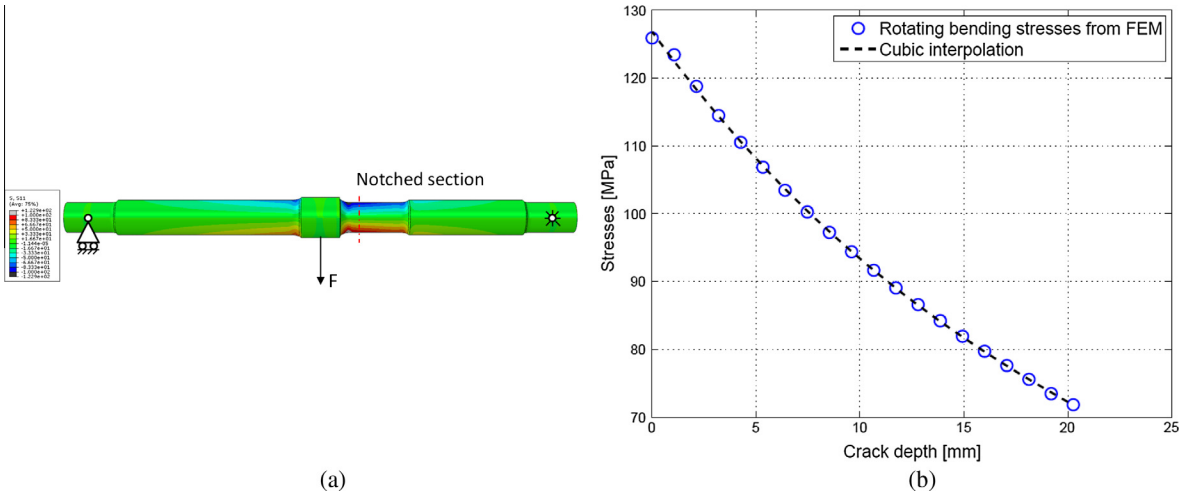

Fig. 10. FE model for the evaluation of the rotating bending stress profile: (a) 3D model of the full-scale specimen; (b) rotating bending stress profile.

experiments. The discrepancy between simulated and experimental results can be explained by the uncertainty about the deepest part of the residual stress profile, which could not be measured. In particular, simulations adopted the exact profile shown in Fig. 4b, which is valid until a 2.5 mm depth, but which also suggests a deeper influence of residual stresses on the growing crack. This means that the slowing effect of compressive residual stresses lasted longer in the tests, increasing the retardation effect on propagation.

Predictions regarding the specimen containing the 4 mm initial notch are shown in Fig. 11c. The CPLR technique is suitably conservative, while the ΔK-decreasing one seems to fit well, suggesting a contradiction with respect to the expected best generating experimental technique for threshold SIF ranges. Indeed, it is worth remembering again that, considering the experiments carried out on EA1N railway steel [32], the best description of threshold SIF values for short and long cracks was gotten by the CPLR technique. Moreover, as highlighted in Section 2, only this technique is able to show, for EA4T, the expected stabilization of threshold SIF ranges below $R = -2$. Considering, instead, variable amplitude loads (for EA4T without deep rolling), a retardation effect was always experimentally observed with respect to constant amplitude ones. In particular, the authors deepen this topic in [48], where it is shown that a simple no-interaction model provides conservative predictions adopting CPLR curves and non-conservative ones adopting ΔK-decreasing data (i.e. experiments show "retardation" with respect to CPLR curves and "acceleration" with respect to ΔK-decreasing ones), while a more sophisticated Strip-Yield model matches the experiments. Also in the present experiments, variable amplitudes loads applied along with deep rolling show a significant retardation and this leads to the impression that ΔK-decreasing data are more suitable. Actually, it is likely that a Strip-Yield prediction could be the best choice again.

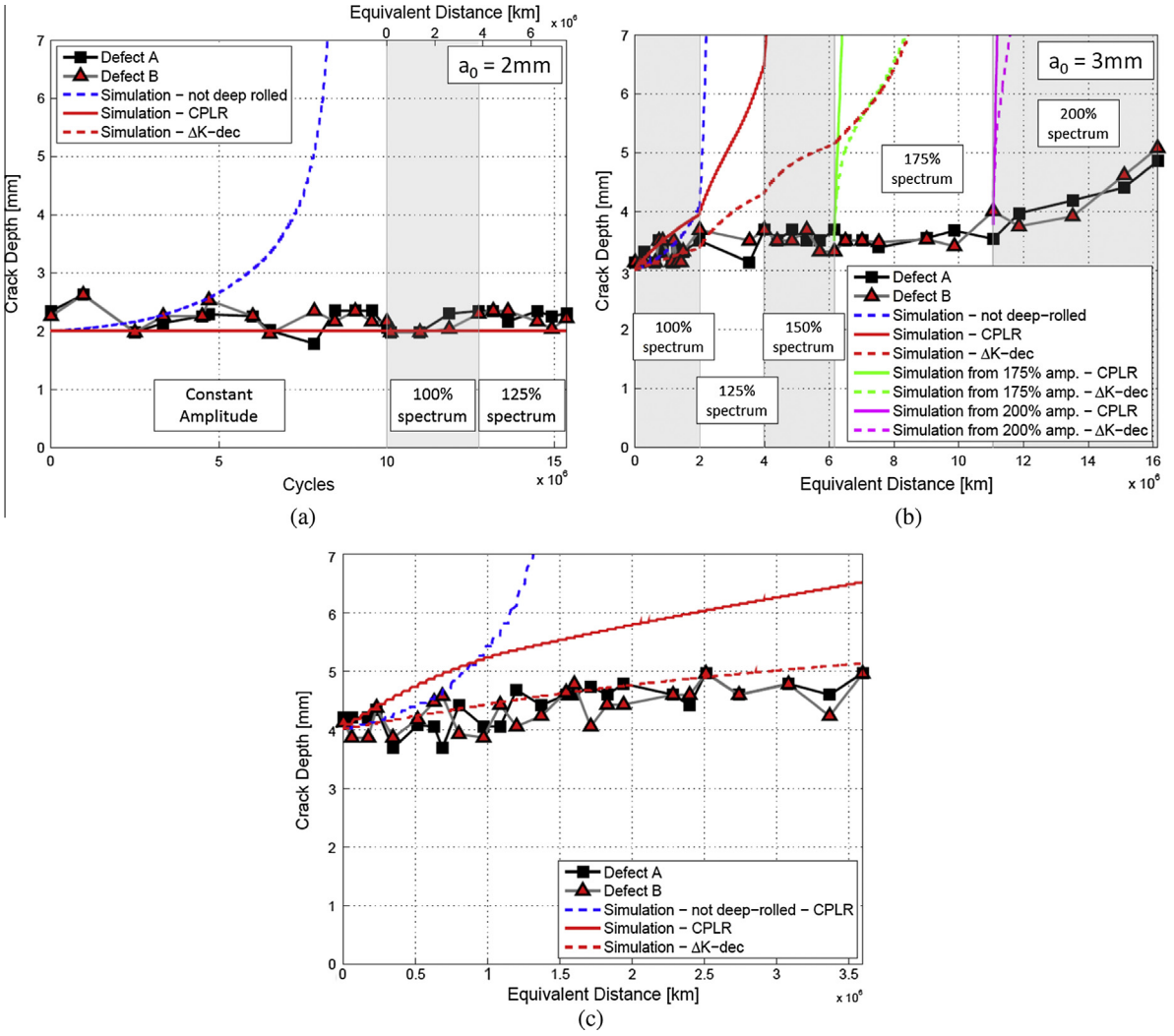

Fig. 11. Crack growth predictions: (a) 2 mm notch; (b) 3 mm notch; (c) 4 mm notch.

Table 2
Simulations of the carried out tests.

Specimen	Test	Cycles	σ_{max} (MPa)	ΔK_{max} (MPa$\sqrt{m}$)	a_0 (mm)	c_0 (mm)	CPLR		ΔK-decreasing	
							Δa (mm)	Δc (mm)	Δa (mm)	Δc (mm)
Specimen #1 $a_0 = 2$ mm	CA	10×10^6	125		2.00	2.00	–	–	–	–
	VA 100%	2.73×10^6		16.70	2.00	2.00	–	–	–	–
	VA 125%	2.62×10^6		20.88	2.00	2.00	–	–	–	–
Specimen #2 $a_0 = 3$ mm	VA 100%	1.43×10^6		20.72	3.00	3.00	0.96	0.05	0.37	–
	VA 125%	1.43×10^6		25.90	3.00	3.00	3.09	1.15	1.21	–
	VA 150%	1.57×10^6		31.08	3.00	3.00	28.05	24.27	2.03	0.04
	VA 175%	3.50×10^6		36.26	3.00	3.00	Failure	15.16	8.83	
	VA 200%	3.57×10^6		41.44	3.00	3.00	Failure	Failure		
Specimen #3 $a_0 = 4$ mm	VA 100%	2.60×10^6		23.80	4.00	4.00	3.52	1.58	1.13	0.01

Finally, results regarding the specimen containing the 4 mm initial notch support the observation made in the case of the 3 mm notch about the uncertainty of the deepest residual stress profile: it likely does not overtake a 4 mm depth, making experiments and simulations similar.

6. Concluding remarks

The effect of deep rolling on propagation lifetime of railway axles was investigated. The relevant results can be summarized:

- Crack growth rates of EA4T grade were experimentally measured at very negative stress ratios, finding a tendency of data to overlap and coincide with those at $R = -2$.
- Three crack propagation tests were carried out on full-scale deep-rolled specimens. Depending on the initial notch size with respect to the depth of compressive residual stresses, no crack initiation could be observed for small flaws ($R = 2$ mm), while unusual crack shape development happened for the largest ones ($R = 3$ mm and $R = 4$ mm).
- A complex surface damage pattern, characterized by crack branching and wide yielded regions, was observed around the tips of the initial notches.
- Considering the case of an initial notch size comparable to the depth of the compressive residual stresses ($R = 3$ mm), crack propagation happened for very high $\Delta K_{max}/\Delta K_{th}$ ratios.
- The compressive residual stress profile due to deep rolling was not modified by the application of a significant number of fatigue cycles.
- Results obtained by a simple no-interaction crack propagation model, taking into account the measured stress field, were successfully compared to full-scale experimental ones.
- A more refined crack propagation model, able to catch the retardation effects of variable amplitude loads along with deep rolling, should be adopted in order to match experimental results on a more robust base.

Acknowledgements

This research was carried out in the frame of the MARAXIL Project co-funded by Regione Lombardia (ID 16973, Rif. no. MAN-15). The authors would like to thank Dr. M. Luke and Dr. I. Varfolomeev (IWM) for the useful help and discussion.

References

[1] EN 13103:2001. Railway applications – wheelset and bogies – non-powered axles – design method. European Committee for Standardization, Technical Committee CEN/TC 25, April; 2001.
[2] EN 13104:2001. Railway applications – wheelset and bogies – powered axles – design method. European Committee for Standardization, Technical Committee CEN/TC 25, April; 2001.
[3] Hoddinot DS. Railway axle failure investigations and fatigue crack growth monitoring of an axle. J Rail Rapid Transit 2004;218:283–92.
[4] Beretta S, Carboni M, Lo Conte A, Palermo E. An investigation of the effects of corrosion on the fatigue strength of A1N axle steel. J Rail Rapid Transit 2008;222:129–43.
[5] Gravier N, Viet JJ, Leluan A. Prédiction de la durée se vie des essieux-axes ferroviaires. Revue générale des chemins de fer 1999;3:33–40.
[6] Grandt Jr AF. Fundamentals of structural integrity. Hoboken, NJ: JohnWiley & Sons; 2004.
[7] Zerbst U, Beretta S, Köhler G, Lawton A, Vormwald M, Beier HTh, et al. Safe life and damage tolerance aspects of railway axles – a review. Engng Fract Mech 2013;98:214–71.
[8] Cantini S, Beretta S (editors), Structural reliability assessment of railway axles. LRS-Techno Series 4; 2011.
[9] Cantini S, Beretta S, Carboni M. POD and inspection intervals of high speed railway axles. In: 15th International wheelset congress, Prague, Czech Republic; 2007.
[10] Carboni M, Beretta S. Effect of probability of detection upon the definition of inspection intervals of railway axles. J Rail Rapid Transit 2007;221:409–17.
[11] Zerbst U, Vormwald M, Andersch C, Mädler K, Pfuff M. The development of a damage tolerance concept for railway components and its demonstration for a railway axle. Engng Fract Mech 2003;72:209–39.
[12] Shot peening applications. 7th ed. Metal Improvement Company Inc., Publication.
[13] Farrahi GH, Lebrijn JL, Couratin D. Effect of shot peening on residual stress and fatigue life of a spring steel. Fatigue Fract Engng Mater Struct 1995;18(2):211–20.
[14] Torres MAS, Voorwald HJC. An evaluation of shot peening, residual stress and stress relaxation on the fatigue life of AISI 4340 steel. Int J Fatigue 2002;24(8):877–86.
[15] Graham H, Hackel LA, Harris F. Surface prestressing to improve fatigue strength of components by laser shot peening. Opt Lasers Engng 2000;34(4):327–37.
[16] Moshier MA, Hillberry BM. The inclusion of compressive residual stress effects in crack growth modeling. Fatigue Fract Eng Mater Struct 1999;22:519–26.
[17] Brennan FP, Ngiam SS, Lee CW. An experimental and analytical study of fatigue crack shape control by cold working. Engng Fract Mech 2008;75:355–63.
[18] Gardin C, Courtin S, Bezine G, Bertheau D, Hamouda H. Numerical simulation of fatigue crack propagation in compressive residual stress fields of notched round bars. Fatigue Fract Engng Mater Struct 2007;30:231–42.
[19] Gardin C, Courtin S, Bertheau D, Bezine G, Hamouda H. The influence of roller burnishing on the fatigue crack propagation in notched round bars – experimental observations under three-point bending, Blackwell Publishing Ltd.. Fatigue Fract Engng Mater Struct 2007;30:342–50.
[20] De los Rios ER, Walley A, Milan MT, Hammersley G. Fatigue crack initiation and propagation on shot-peened surfaces in A316 stainless steel. Int J Fatigue 1995;17(7):493–9.
[21] Song PS, Wen CC. Crack closure and crack growth behavior in shot peened fatigued specimen. Engng Fract Mech 1999;63(3):295–304.
[22] Hatamleh O, Lyons J, Forman R. Laser and shot peening effects on fatigue crack growth in friction stir welded 7075-T7351 aluminum alloy joints. Int J Fatigue 2007;29(3):421–34.
[23] Altenberger I, Scholtes B, Martin U, Oettel H. Cyclic deformation and near surface microstructures of shot peened or deep rolled austenitic stainless steel AISI 304. Mater Sci Engng 1999;A264(12):1–16.

[24] Nalla RK, Altenberger I, Noster U, Liu GY, Scholtes B, Ritchie RO. On the influence of mechanical surface treatments - deep rolling and laser shock peening – on the fatigue behavior of Ti–6Al–4V at ambient and elevated temperatures. Mater Sci Engng 2003;A355(12):216–30.
[25] Altenberger I. Deep rolling – the past, the present and the future. In: Proceedings of 9th international conference on shot peening; 2005. p. 6–9.
[26] MARAXIL project. <http://maraxil.mecc.polimi.it/>; 2013. (accessed on 05.12).
[27] Forman R, McClung RC. NASGRO 4.0, fracture mechanics and fatigue crack growth analysis software, reference manual. Southwest Research Institute; 2002.
[28] UNI EN 13261:2011. Railway application – wheelsets and bogies – axles – product requirements, CEN; 2010.
[29] Forth SC, Newman Jr J, Forman RG. On generating fatigue crack growth thresholds. Int J Fatigue 2003;25:9–15.
[30] Forth SC, Newman J, Jr., Forman RG. Evaluation of fatigue crack thresholds using various experimental methods. ASTM Special Technical Publication, 1461, p. 203.
[31] Newman Jr J, Schneider J, Daniel A, McKnight D. Compression pre-cracking to generate near threshold fatigue-crack-growth rates in two aluminium alloys. Int J Fatigue 2005;27:1432–40.
[32] Carboni M, Patriarca L, Regazzi D. Determination of ΔK_{th} by compression pre-cracking in a structural steel. J ASTM Int 2009;6(9):1–13.
[33] ASTM E647-05. Standard test method for measurement of fatigue crack growth rates. Annual book of ASTM standards. ASTM International; 2005, vol. 3, p. 1.
[34] Pippan R. The growth of short cracks under cyclic compression. Fatigue Fract Engng Mater Struct 1987;9:319–28.
[35] Newman J, Jr., Yamada Y. Compression pre-cracking methods to generate near-threshold fatigue-crack-growth-rate data. In: 17th European conference on fracture (ECF17), Brno, Czech Republic; 2008.
[36] Pippan R, Stüwe HP, Golos K. A comparison of different methods to determine the threshold of fatigue crack propagation. Fatigue 1994;16:579–82.
[37] Nelson W. Applied life data analysis. New York: J. Wiley & Sons; 1981.
[38] Carboni M, Regazzi D. Effect of the experimental technique onto R dependence of ΔK_{th}. Proc Engng 2011;10:2937–42.
[39] Beretta S, Carboni M, Cervello S. Design review of a freight railway axle: fatigue damage versus damage tolerance. Mat-wiss U Werkstofftech 2011;42:12.
[40] Swain MH. Monitoring small crack growth by the replication method. ASTM STP 1149; 1992.
[41] Krautkrämer J, Krautkrämer H. Ultrasonic testing of materials. Springer-Verlag; 1990.
[42] Hauk V. Structural and residual stress analysis by nondestructive methods. Elsevier; 1997.
[43] NPL. Measurement good practice guide N. 52 determination of residual stresses by X-ray diffraction; 2002 [ISSN 1368–6550].
[44] Hassani-Gangaraj SM, Carboni M, Guagliano M. On the generation of residual stresses in railway axles made of a medium strength steel and processed by deep rolling. Mater Des; 2014 [submitted for publication].
[45] Regazzi D. Advances in life prediction and durability of railway axles. PhD thesis. Politecnico di Milano.
[46] Shiratori M, Miyoshi T, Tanikawa K. Analysis of stress intensity factors for surface cracks subjected to arbitrarily distributed surface stresses. Trans Jpn Soc Mech Eng 1986;52:409–17.
[47] Madia M, Beretta S, Schödel M, Zerbst U, Luke M, Varfolomeev I. Stress intensity factor solutions for railway axles. Engng Fract Mech 2011;78:764–92.
[48] Beretta S, Carboni M, Regazzi D. Load interaction effects in a medium strength steel for railway axles. Mater Perform Charact; 2014.